

GenPlan: Generative Sequence Models as Adaptive Planners

Akash Karthikeyan¹, Yash Vardhan Pant¹

¹University of Waterloo, Canada
 {a9karthi, yash.pant}@uwaterloo.ca

Abstract

Sequence models have demonstrated remarkable success in behavioral planning by leveraging previously collected demonstrations. However, solving multi-task missions remains a significant challenge, particularly when the planner must adapt to unseen constraints and tasks, such as discovering goals and unlocking doors. Such behavioral planning problems are challenging to solve due to: a) agents failing to adapt beyond the single task learned through their reward function, and b) inability to generalize to new environments, e.g., those with walls and locked doors, when trained only in planar environments. Consequently, state-of-the-art decision-making methods are limited to missions where the required tasks are well-represented in the training demonstrations and can be solved within a short (temporal) planning horizon. To address this, we propose GenPlan: a stochastic and adaptive planner that leverages discrete-flow models for generative sequence modeling, enabling sample-efficient exploration and exploitation. This framework relies on an iterative denoising procedure to generate a sequence of goals and actions. This approach captures multi-modal action distributions and facilitates goal and task discovery, thereby generalizing to out-of-distribution tasks and environments, i.e., missions not part of the training data. We demonstrate the effectiveness of our method through multiple simulation environments. Notably, GenPlan outperforms state-of-the-art methods by over 10% on adaptive planning tasks, where the agent adapts to multi-task missions while leveraging demonstrations from single-goal-reaching tasks. Our code is available at <https://github.com/CL2-UWaterloo/GenPlan>.

1 Introduction

An intelligent autonomous agent must be adaptable to new tasks at runtime beyond those encountered during training. This is crucial for operating in complex environments that may introduce distractors (i.e., objects the agent has not seen before) and have multiple novel goals.

Example 1 Consider a task where an agent is initially trained on a simple single-goal-reaching task in a planar environment. During evaluation, the agent must adapt to complex environments with walls, locked doors, and multiple goals, as illustrated in figure 1A. The planner must generate multi-step trajectories, exploring to locate goals

Copyright © 2025, Association for the Advancement of Artificial Intelligence (www.aaai.org). All rights reserved.

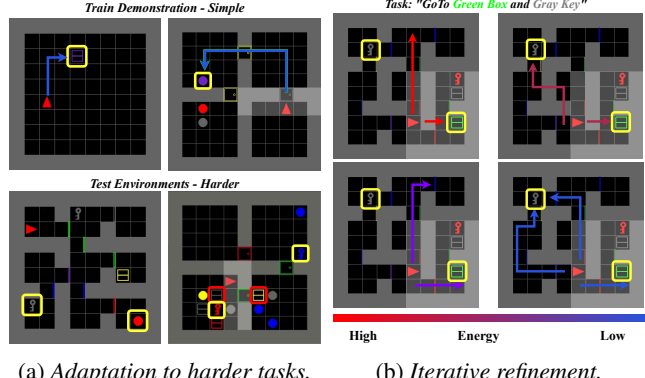


Figure 1: Overview. GenPlan is a generative, multi-step planner that optimizes energy landscape to adapt to complex tasks and iteratively refine long-horizon missions. Goals are highlighted in yellow, and distractors are marked in red.

while avoiding getting stuck, unblocking paths, and navigating around walls to complete the mission.

Learning such behaviors from demonstrations is challenging and often requires a diverse dataset that accurately represents the necessary tasks. This is much harder for long-horizon tasks, where the correct order of subtasks is critical (e.g., collecting a key before unlocking a door).

Reinforcement learning via Supervised Learning (RvS) (Emmons et al. 2022) simplifies traditional Reinforcement Learning (RL) by using a behaviour cloning (BC) objective and framing RL as sequence modeling, where actions are sequentially predicted based on next best action. However, this approach often struggles in order-critical multi-task missions, as generated plans can suffer from locally optimal decisions, resulting in global dead-ends, or accumulate errors without accounting for mistakes in previous actions (Lambert, Pister, and Calandra 2022).

Thus, a categorical distribution is better suited for capturing abstracted sequence planners (Lee et al. 2024), as it enables clustering of different modes and provides interpretable predictions of subtask orders. More recently, generative modeling-based works allow conditional sequence-level predictions (Janner et al. 2022; Chi et al. 2023). However, based on our results evaluating energy models and

diffusion methods with various objectives (e.g., BC) and sampling techniques, such as the cross-entropy method, Gibbs sampling, and energy gradient-based guidance, these approaches fail on multi-step planning (discrete) see Appendix C. They often get stuck in local optima when handling unseen cases, as they lack distributional fidelity and struggle to adapt to new tasks.

Contributions of this work. To address these challenges, we propose GenPlan, a discrete flow-based framework for sequence modeling that utilizes a Continuous Time Markov Chain (CTMC)-based sampling method. Our key contributions are as follows:

- GenPlan frames planning as the iterative denoising of trajectories using discrete flow models. This approach enables adaptability by allowing goal and task discovery.
- Learn an energy function to guide denoising and minimize it to generate action sequences.
- GenPlan uses an entropy-based lower bound over action probabilities to encourage adaptability and generalization to previously unseen tasks and environments.

Thus, instead of greedily selecting the next action, GenPlan jointly learns goal and action distributions with bi-directional context. This approach prevents the agent from stalling and getting stuck in local regions. Additionally, framing planning as generative modeling, GenPlan allows for generalization to novel environments, as long as the objective function remains consistent (i.e., assigning minimal energy to successful trajectories). Through extensive simulations, we empirically demonstrate that GenPlan outperforms state-of-the-art models by over 10% in adaptive planning, particularly in challenging environments with multiple sub-goals, while only leveraging demonstrations from single-goal-reaching tasks.

2 Related Works

Offline RL. Offline RL focuses on learning policies from collected demonstrations, as illustrated in figure 2A, without further interaction with the environment (Levine et al. 2020). A key challenge in this approach is the *distribution shift* between the training demonstrations and the runtime distribution. Several regularization strategies have been proposed to address this, such as reducing the discrepancy between the learned and behavioral policies (Fujimoto, Meger, and Precup 2019; Kumar et al. 2019). However, these approaches often fail to adapt to unseen tasks and are typically limited to single-step planning. We are interested in optimizing sequence-level plans.

More recent works (Chen et al. 2021; Janner, Li, and Levine 2021; Furuta, Matsuo, and Gu 2022) adopt an autoregressive modeling objective, leveraging the self-attention mechanism of sequence models. By conditioning on desired returns or goal states, these methods guide the generation of future actions, provided such states are encountered during training. While effective for behavior cloning tasks, they fail in scenarios like Example 1 due to deadlocks. Moreover, they struggle in unconditional rollouts, lacking both guidance and the ability to generalize to novel goals.

Planning with Sequence Models. Planning Transformer (Sun et al. 2022) introduces procedural planning with transformers by framing planning as a model-based RL problem. It employs a joint action and state representation model to mitigate compounding errors inherent in transformer-based architectures. LEAP (Chen et al. 2023) addresses planning as an iterative energy minimization problem, utilizing a Masked Language Model (MLM) to learn trajectory-level energy functions. This approach employs Gibbs sampling prevents error accumulation and demonstrates generalization to novel test scenarios. However, LEAP’s reliance on an oracle for goal positions limits its effectiveness, particularly in larger mazes, as shown in our simulation studies (see Table 1). Without conditional guidance, performance declines significantly. This limitation can cause the agent to enter loops, leading to *stalling actions*, where it fails to make progress.

Generative Models in Planning. Deep generative models have recently demonstrated success in offline RL. Broadly, energy-based models (Haarnoja et al. 2017; Eysenbach et al. 2022) and diffusion models (Janner et al. 2022; Chi et al. 2023) have been applied to offline RL tasks. While diffusion-based models often require well-represented datasets, they fail to generalize to unseen harder tasks, as shown in figure 1A. In contrast, energy-based models can learn an energy landscape that helps generalize to unseen tasks; however, they are challenging to sample from, requiring cross-entropy or MCMC sampling (Chen et al. 2023), and are often unstable to train (Chi et al. 2023). Recently, energy-diffusion(Du, Mao, and Tenenbaum 2024) proposes guided diffusion sampling with energy gradients. However, in planning tasks, we observed that the low-energy trajectories can be gamed by repetitive frequent actions from the demonstrations (e.g., forward actions), causing the model to get trapped in local minima.

To address these challenges, we propose an energy-diffusion framework (GenPlan) capable of iteratively refining plans for unseen environments by learning annealed energy landscapes and employing diffusion-based sampling to enable goal and task discovery.

3 Preliminaries and Problem Statement

Notations. We model discrete data as a sequence (x_1, \dots, x_H) , where H is the horizon. This sequence is represented by \mathbf{x} , with each x_k denoting a step in the sequence. The superscript x^t indicates the time step in the CTMC, with $t \in [0, 1]$. Each $x_k^t \in X$ takes a discrete value from the set $X = \{1, \dots, x_{|X|}\}$, with $|X|$ denoting the cardinality of this set. This notation applies to any discrete variable, such as a state s or an action a . We denote the dataset by \mathcal{D} , representing a collection of demonstrations. We use \mathcal{C} and \mathcal{U} to denote categorical and uniform distributions, respectively. Additionally, we utilize $\delta\{i, j\}$ to represent the Kronecker delta, which equals 1 when $i = j$ and 0 otherwise.

Reinforcement Learning. We extend the standard Markov Decision Processes (MDP) framework by incorporating a sequence of goals $G = \{g_1, \dots, g_n\}$ within the

state space S . Formally, we consider learning in a MDP $\mathcal{M} = \langle S, A, P, R \rangle$. The MDP tuple comprises S and A to denote the state and action spaces, respectively, with discrete states $s_k \in S$ and actions $a_k \in A$. The transition function $P(\cdot|s_k, a_k)$ returns a probability distribution over the next states given a state-action pair. The reward function R provides a binary reward $r_k(s_k, a_k, s_{k+1}) = \mathbb{I}\{s_{k+1} \in G\}$. The aim is to learn a policy $\pi_\theta(a_k|s_k)$ that maximizes cumulative rewards. While this approach allows for policy optimization, it is often restricted to single-step rollouts. In contrast, we focus on a multi-step planning framework that enables planning over a longer horizon, avoiding locally optimal decisions that may lead to global dead-ends.

RL as sequence modeling. Decision Transformer (DT) (Chen et al. 2021) frames RL as a sequence modeling problem, allowing training through upside-down RL (Schmidhuber 2020) in a supervised manner. Given a dataset $\mathcal{D} = \{\tau_i \mid 1 \leq i \leq N\}$ of near-optimal trajectories collected through demonstrations, where each trajectory $\tau_i = (s_1, a_1, g_1, \dots, s_H, a_H, g_H)$ has a length H , DT aims to train an agent π_θ by minimizing the cross-entropy loss $\mathcal{L}_{\text{CE}}(\hat{a}, a)$ between the predicted actions \hat{a} and the true actions a in the demonstrations. Although this BC-based approach has been successful in causal inference tasks (e.g., robotics), it lacks the ability for sequential refinement and is prone to error accumulation. Our approach addresses these limitations by integrating sequence models with an iterative denoising method for more efficient multi-step planning.

Discrete Flow Model (DFM). For simplicity, we assume $H = 1$. However, this can be extended to multidimensional data by employing factorization assumptions, as demonstrated in (Campbell et al. 2024). Consider the probability flow p_t as marginal distribution of x^t (samples in the CTMC). The objective of generative flow models is to transform source (noise) samples $p_0(x^0) = p_{\text{noise}}(x^0)$ to target (data) samples $p_1(x^1) = p_{\text{data}}(x^1)$. The probability that x^t will jump to other states j is determined by a rate matrix $R_t \in \mathbb{R}^{|X| \times |X|}$. Thus, we can represent the transition probabilities for an infinitesimal time dt :

$$p_{t+dt|t}(j|x^t) = \begin{cases} R_t(x^t, j)dt & \text{for } j \neq x^t \\ 1 + R_t(x^t, x^t)dt & \text{for } j = x^t \end{cases} \quad (1)$$

$$= \delta\{x^t, j\} + R_t(x^t, j)dt \quad (2)$$

where $\delta\{i, j\}$ equals 1 when $i = j$ and 0 otherwise. We define a forward corruption process (data-to-noise interpolation) as $p_t(x^t) = \mathbb{E}_{p_{\text{data}}(x^1)} [p_{t|1}(x^t|x^1)]$, with p_t represented by the conditional flow $p_{t|1}(\cdot|x^1)$. We consider two types of interpolants: masking-based and uniform noise, both modeled as categorical distributions (\mathcal{C}):

$$p_{t|1}^{\text{mask}}(x^t | x^1) = \mathcal{C} (t\delta\{x^1, x^t\} + (1-t)\delta\{[M], x^t\}) \quad (3a)$$

$$p_{t|1}^{\text{unif}}(x^t | x^1) = \mathcal{C} \left(t\delta\{x^1, x^t\} + (1-t)\frac{1}{|X|} \right) \quad (3b)$$

Here, $[M]$ represents a mask state (Devlin et al. 2018) and $\frac{1}{|X|}$ denotes uniform prior. To simulate the reverse flow (interpolation from noise to data), we need to determine the

rate matrix R that generates these marginals. This is expressed as $\partial_t p_t(\cdot) = R_t(\cdot|\cdot)^\top p_t$. Campbell et al. (2024) proposes the use of a conditional rate matrix, $R_t(x^t|j) = \mathbb{E}_{p_{1|t}}[R_t(x^t, j|x^1)]$, which enables the simulation of the conditional flow, by sampling along CTMC.

Learning a denoising model. The $p_{1|t}$ term is analytically intractable, but it can be approximated using a neural network with parameters θ , and this model is commonly referred to as a denoising model ($p_{1|t}^\theta$) in literature.

Challenges. Given an offline dataset, we wish to learn a planner that allows for sampling multi-step plans for a given task and environment. Primarily, we wish to address the following challenges: (1) Unconditional trajectory generation (goal position not available to the planner). (2) Even when goals are specified, goal-conditioned trajectories may provide insufficient guidance for long-horizon tasks, especially when the goal position is far from the agent’s current position. (3) The agent may fail to adapt to multi-goal settings (harder) at test time, as BC-based objectives result in memorization and are prone to accumulating errors over a long planning horizon. (4) Need for stochasticity in the planner, as we may encounter tasks previously unencountered (e.g., door-unlocking tasks) or unfamiliar environments (e.g., mazes).

4 GenPlan: Method

Overview. The denoising planner integrates the DFM with sequence models and is built on two key components: (a) the denoising model $p_{1|t}^\theta$, trained as described in algorithm 1, and (b) the rate matrix $R_t(x^t, x^t|x^1)$. Together, these components enable flexible planning using the algorithm 2. We discuss several design choices that improve the planner’s performance. For further details on the implementation and the formulation of the rate matrix, refer to Appendix F.

Energy-Guided Denoising Model

Given demonstrations (see Section 3), our aim is to learn an implicit energy function for a sequence, denoted as $\mathcal{E}(\mathbf{a}^t)$. This energy function is designed to assign lower energy to optimal action sequences. We define the energy as the sum of negative pseudo-likelihood over the horizon, formulated as $\mathcal{E}(\mathbf{a}^1) = \mathbb{E}_{(\mathbf{a}^1) \sim \mathcal{D}} \sum_H [-\log p_{1|t}^\theta(\mathbf{a}^1 | \mathbf{a}^0, \mathbf{o})]$ adapted from (Goyal, Dyer, and Berg-Kirkpatrick 2021).

Our approach leverages the DFM objective (Campbell et al. 2024, 2022) to learn a locally normalized energy score. This score allows us to evaluate generated rollouts and frame planning as an iterative denoising process. Energy guidance ensures that the optimization process stays at an energy minimum at each step (Goyal, Dyer, and Berg-Kirkpatrick 2021; Chen et al. 2023). The denoiser $p_{1|t}^\theta$ is optimized under the constraint that its entropy \mathcal{H} remains above a lower bound β . This constraint encourages stochasticity, enhancing the gen-

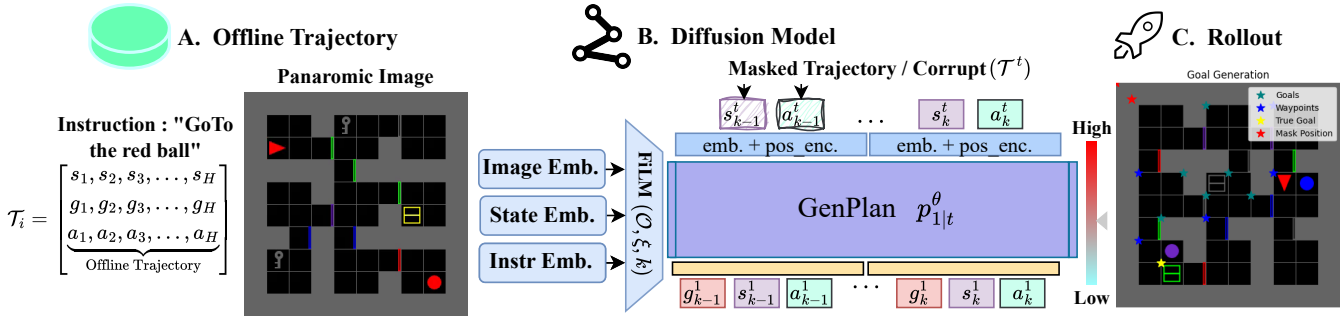


Figure 2: **Method Overview.** GenPlan, trained on offline data (A), learns to jointly model action, goal, and state distributions. In (B), the joint denoising model (see Section 4) takes in a corrupted trajectory τ^t and predicts the clean trajectory τ^1 . (C) Demonstrates the joint inference of goals and actions by simulating the reverse CTMC, as detailed in Algorithm 2.

erative model’s adaptability to new tasks and environments.

$$\min_{\theta} \mathbb{E}_{\mathbf{a}^0 \sim p_0, \mathbf{o} \sim \mathcal{D}} \left[\sum_{k=1}^H -\log p_{1|t}^\theta(\mathbf{a}^1 | \mathbf{a}^0, \mathbf{o}) \right], \quad (4a)$$

$$\text{s.t. } \mathbb{E}_{\mathbf{a}^0 \sim p_0, \mathbf{o} \sim \mathcal{D}} \left[\sum_{k=1}^H \mathcal{H}(p_{1|t}^\theta(\mathbf{a}^1 | \mathbf{a}^0, \mathbf{o})) \right] \geq \beta \quad (4b)$$

By optimizing at the sequence level, the model avoids getting trapped in local minima and can naturally learn a multi-modal distribution, where $\mathcal{E}(\mathbf{a}) \simeq \mathcal{E}(\mathbf{a}')$, finding multiple viable solutions. This framework enables the flexible formulation of RL and planning tasks. In Section 5, we demonstrate the use of a joint model (Section 4) for generating unconditional rollouts.

Joint Denoising Model

Goal Generation. GenPlan addresses complex planning tasks by using instruction prompts or the environment’s observations to define objectives. We achieve this by learning a goal distribution conditioned on observations \mathbf{o} , which guides the action denoising process. Unlike existing methods (Chen et al. 2021, 2023) that rely on simulators for runtime goal positions and task proposals, GenPlan jointly learns the goal distribution, extracting a goal sequence \mathbf{g} jointly with actions \mathbf{a} during planning. This dynamic goal proposal promotes exploration and improves performance in long-horizon tasks by reducing error accumulation.

State Sequence. In addition to goal generation, we also learn a state denoising model. We found that goal conditioning becomes ambiguous when the proposed goal is far from the agent’s position. To prevent the agent from stalling or getting stuck in local regions, we learn the state sequence, which further aids in learning the action distribution.

These auxiliary modules are trained similarly to the action sequence (denoising based DFM) and can generalize to out-of-distribution tasks, provided the energy function is generalizable—successful trajectories receive low energy. Next, we briefly describe the processes involved in training and sampling from DFM (Campbell et al. 2024, 2022).

Forward Diffusion. We begin by corrupting samples drawn from the dataset \mathcal{D} using the noise schedules (eq. 3a,3b). Specifically, we apply $\mathbb{E}_{p_{\text{data}}(\tau^1), t \sim \mathcal{U}[0,1]} p_{t|1}^{\text{mask}}(\tau^t | \tau^1)$, where t is the CTMC timestep that controls the amount of corruption. The corruption process is applied to \mathbf{s} , \mathbf{a} , and \mathbf{g} , with the jump rate controlled by t . This training is independent of the rate matrix, offering greater flexibility during inference.

Backward Diffusion. The denoising objective is applied at the trajectory level, making the transition from noise to data distribution challenging, particularly for longer horizons. This requires an iterative process. Using the corrupted tokens as input, we train the joint denoising model ($p_{1|t}^\theta$) to approximate the true data distribution. We employ a negative-log-likelihood-based loss (eq. 5) to predict \mathbf{s}^1 , \mathbf{g}^1 , and \mathbf{a}^1 . As noted in (Campbell et al. 2024), the denoiser $p_{1|t}^\theta(\tau^1 | \tau^t)$ is independent of the choice of rate matrix used for sampling, $R_t(\mathbf{x}^t, \mathbf{x}^{t'} | \mathbf{x}^1)$. This offers flexibility during sampling and simplifies the training. Following algorithm 2, we can sample the reverse CTMC to generate rollouts.

Observation Conditioning. We employ a transformer-style architecture (Chen et al. 2021), using bi-directional masks as in (Devlin et al. 2018) to allow future actions to influence preceding ones. Observations \mathbf{o} are encoded using FiLM (Feature-wise Linear Modulation) (Perez et al. 2018) to process images I , instruction prompts ξ , and agent positions. The context length is typically set to 1 but can be extended to increase the agent’s memory (see figure 2B).

Training Objective

The training objectives described in eq. 4a,4b are used to learn the model parameters (θ, λ) . Here, θ represents the parameters of the denoiser $p_{1|t}^\theta$, which is parameterized as a transformer, as discussed in Section 4. The parameter $\lambda \in [0, \infty]$ is the Lagrangian multiplier associated with the constraints in eq. 4b. We alternate gradient descent steps between updating $p_{1|t}^\theta$ and λ . In practice, $\lambda \rightarrow 0$, ensuring that the lower bound β on entropy is satisfied (Zheng, Zhang, and Grover 2022). To generalize the denoiser across differ-

Algorithm 1: GenPlan Training

```

1: init denoiser  $p_{1|t}^\theta$ ,  $\tau^0 \sim p_{\text{noise}}$ ,  $\beta = 0.5$ ,  $\text{maxiters} = 5k$ 
2: for  $i$  in  $\text{maxiters}$  do
3:    $t \sim \mathcal{U}[0, 1]$ ,  $\tau^1 \sim \mathcal{D}$ ,  $\mathbf{o} \sim \mathcal{D}$ 
4:    $p_{t|1}^{\text{mask}}(\tau^t | \tau^1)$  // see eq. 3a
5:    $\mathcal{L}_{\text{NLL}} \leftarrow \mathcal{L}_a + \mathcal{L}_s + \mathcal{L}_g$  // see eq. 5
6:    $\mathcal{L}_{\text{ent}} \leftarrow \mathbb{E}_{\mathbf{a} \sim \mathcal{D}} [\mathcal{H}(p_{1|t}^\theta(\mathbf{a} | \tau^0, \mathbf{o}))]$  // see eq. 4b
7:    $\mathcal{L}_\pi(\theta) = \mathcal{L}_{\text{NLL}} - \lambda \mathcal{L}_{\text{ent}}$ 
8:    $\theta \leftarrow \theta - \nabla_\theta \mathcal{L}_\pi(\theta)$ 
9:    $\lambda \leftarrow \lambda - (\mathcal{H}[p_{1|t}^\theta(\cdot | \tau^0, \mathbf{o})] - \beta)$ 
10: end for

```

ent levels of corruption, we train the model to recover trajectories with varying noise levels. For each $\langle \mathbf{a}, \mathbf{s}, \mathbf{g} \rangle$, we apply the loss \mathcal{L}_x (see eq. 5). The Kronecker delta ensures that the loss is only calculated for the corrupted regions.

$$\mathcal{L}_x = \left[- \sum_{k=1}^H \delta\{x_k^t, [\mathbf{M}]\} \log p_{1|t}^\theta(\mathbf{x}^1 | \mathbf{x}^t, \mathbf{o}) \right] \quad (5)$$

Planning

Once the denoising model has been trained, we can generate trajectories that approximate the data distribution by reversing the CTMC and interpolating noise back into the data through iterative denoising (I_{max} iterations). The following algorithm outlines this process, based on the approach in (Campbell et al. 2024). This procedure is applied to all components of the trajectories.

Algorithm 2: GenPlan Sampling

```

1: init  $\tau^0 \sim p_0$ , choice of  $R_t(\tau^t, \cdot | \tau^1)$ ,  $\Delta t = \frac{1}{I_{\text{max}}}$ , get  $\mathbf{o}$ 
2: for  $t \in \{0, \Delta t, 2\Delta t, \dots, 1\}$  do
3:    $R_t^\theta(\tau^t, \cdot) \leftarrow \mathbb{E}_{p_{1|t}^\theta(\tau^1 | \tau^t, \mathbf{o})} [R_t(\tau^t, \cdot | \tau^1)]$ 
4:    $\tau^{t+\Delta t} \sim \mathcal{C}(\delta\{\tau^t, \tau^{t+\Delta t}\} + R_t^\theta(\tau^t, \tau^{t+\Delta t}) \Delta t)$ 
5:    $t \leftarrow t + \Delta t$ 
6: end for
7: return  $\mathbf{a}, \mathbf{s}, \mathbf{g}$  // extract from  $\tau^1$ 

```

Remark 1 *Extending rate matrices to sequences:* For multidimensional input, line 4 of algorithm 2 factorizes $\mathcal{C}(\cdot)$ as shown below. This is due to the following reasons: (1) The corruption process is independent across the horizon, meaning R_t^k depends only on x_k^t , j_k , and x_k^1 . (2) Once the process reaches x_k^1 , it remains there, i.e., $R_t^k(x_k^t = x_k^1, j_k | x_k^1) = 0$.

$$\delta\{\mathbf{x}^t, \mathbf{x}'^t\} + \sum_{k=1}^H \delta\{\mathbf{x}_k^t, \mathbf{x}'_k^t\} \mathbb{E}_{p_{1|t}^\theta(x_k^1 | \mathbf{x}^t)} [R_t^k(x_k^t, j_k | x_k^1)] \Delta t$$

5 Simulation Studies

We evaluate the performance of GenPlan in BabyAI (Chevalier-Boisvert et al. 2019) and continuous manipulation tasks, focusing on the agent's adaptive and generalization capabilities. We implemented GenPlan

using Python 3.8 and trained it on a 12-core CPU alongside an RTX A6000 GPU.

BabyAI

BabyAI offers a diverse set of tasks and environments (discrete) focused on planning and task completion.

Simulation Setup. We conduct simulations in a modified BabyAI suite following three paradigms.

- Trajectory Planning (TP).** The agent navigates to one or more goals in a maze world, with map layouts, agent initialization, and goal positions varied in each run, evaluating GenPlan's generalization.
- Instruction Completion (IC).** The agent operates in a multi-objective environment requiring complex decision-making, including *exploration, object manipulation, key collection, and sequential goal completion*. Task order and navigation are critical.
- Adaptive Planning (AP).** The model, trained on simple goal-reaching tasks, is evaluated for zero-shot adaptation across harder environments without additional fine-tuning. This includes testing the agent in increasingly complex environments, such as mazes with multiple goals and closed doors, where the agent must demonstrate door-opening and navigation skills. Additionally, we assess the model's ability to adapt to environments in which obstacles must be unblocked to succeed.

To navigate and interact with the environment, the agent can choose from six actions: *left, right, forward, open, drop, or pick up*. Success rates in reaching goals and completing tasks are reported across 250 novel environments. The map layout, goals, obstacles, and agent positions are randomized in each run. As described in Section 4, the planner uses an image observation and instruction to denoise the action sequences. Further details on the environment, baseline configurations, and implementation are provided in Appendix A.

Baselines. We evaluate both versions of GenPlan, named GenPlan-M (GP-M) and GenPlan-U (GP-U), corresponding to the masked and uniform noise variants, respectively. These are compared against several baselines:

- LEAP** (Chen et al. 2023): A MLM based multi-step planner, which has access to simulator-based goal-conditioning for sub-goals.
- LEAP \ominus GC**: A variant of LEAP where simulator access is removed to evaluate its unconditional rollouts.
- DT** (Chen et al. 2021): Utilizes a causal transformer for planning, also with simulator-based goal-conditioning.

While DT and LEAP could learn goal distributions, the MLE objective suffers from poor generalization, often predicting goal positions as corner cells. In contrast, the generative objective combined with DFM sampling in GenPlan demonstrates superior generalization (figure 2C). To improve competitiveness, baselines with simulator access to goal positions are categorized as conditional rollouts, while those relying on instructions and images to recover successful tra-

Env.	Uncond. Rollouts			Cond. Rollouts	
	GP-U	GP-M	LEAP \ominus GC	LEAP	DT
Traj. Planning (TP)					
MazeS4G1	52.4%	62%	44%	49.2%	46.8%
MazeS4G2	38.8%	39.6%	20%	37.6%	35.2%
MazeS7G1	45.6%	44.8%	12%	33.2%	40%
MazeS7G2	21.2%	19.6%	3.6%	4%	13.6%
TP (7.6 \uparrow)	39.5%	41.5%	19.9%	31%	33.9%
Instr. Completion (IC)					
MazeClose	42.8%	48.4%	18%	38.8%	40%
DoorsOrder	40.8%	35.2%	11.2%	36.4%	40.8%
BlockUn	13.2%	16%	0%	0.8%	0%
KeyCorS3R3	11.6%	17.6%	0%	0.4%	3.6%
IC (8.2 \uparrow)	27.1%	29.3%	7.25%	19.1%	21.1%

Table 1: **BabyAI quantitative performance.** Success rates of the models across different environments are presented. The abbreviations **SW**, **NX**, **RY**, and **GZ** in the environment names represent the size (**W**) of a room in the map, the number of obstacles (**X**), the number of rows (**Y**), and the number of goals (**Z**) during testing, respectively. The term “*Close*” indicates that the agent requires door-opening actions.

jectories are categorized as unconditional rollouts. Comparative results are presented in Tables 1 and 2.

Remark 2 *LEAP outperforms popular baselines, including model-free RL algorithms like Batch-Constrained Deep Q-Learning (Fujimoto, Meger, and Precup 2019) and Implicit Q-Learning (Kostrikov, Nair, and Levine 2021), as well as model-based RL methods such as the Planning Transformer (Sun et al. 2022) and Model-based Offline Policy (Yu et al. 2020), in single-goal tasks within BabyAI environments, as shown in Table 1 of LEAP (Chen et al. 2023).*

Results. GenPlan consistently achieves higher success rates, particularly in adaptive planning and long-horizon tasks, as shown in Table 1. Success rates decline as environments grow or involve multiple goals (e.g., **MazeS7G2**), reflecting the challenges of multi-step planning, where committing to incorrect plans results in deadlocks. GenPlan succeeds in complex, order-critical multi-task missions that require completing sub-tasks (e.g., key collection, obstacle unblocking) to achieve higher-level objectives, where baselines fail, particularly in **KeyCorS3R3** and **BlockUn**. In tasks requiring strict task order (e.g., **DoorsOrder**), DT performs comparably due to simulator access for correct goal sequencing, while GenPlan relies solely on instruction embedding as seen in Section 4.

Next, we assess the model’s adaptation capabilities in novel environments (see Table 2). Initially trained in a simple, single-goal plane world task, the model is then evaluated on increasingly challenging tasks. Through the joint denoising process, GenPlan can eventually find a plan given enough timesteps as long as the energy function generalizes well. The goal-generation module allows dynamic updates of sub-goals, aiding exploration, while the entropy regularizer helps the model learn new skills, such as obsta-

Environment	Uncond. Rollouts			Cond. Rollouts	
	GP-U	GP-M	LEAP \ominus GC	LEAP	DT
Adaptive Planning (AP)					
LocS10N10G2	82.4%	88%	76%	78%	25.6%
MazeS4N3G1	56%	62%	44.8%	48%	24%
MazeClose	31.2%	34.8%	10%	10%	8.8%
MazeS4G2	28.8%	34.8%	14%	18.4%	3.6%
SeqS5R2Un	35.6%	42%	29.2%	38%	29.2%
AP (13.84 \uparrow)	46.8%	52.3%	34.8%	38.4%	18.2%

Table 2: **BabyAI quantitative performance.** Success rates of the models across different environments are presented. The abbreviations **SW**, **NX**, **RY**, and **GZ** in the environment names represent the size (**W**) of a room in the map, the number of obstacles (**X**), the number of rows (**Y**), and the number of goals (**Z**) during testing, respectively.

cle unblocking, even without explicit demonstrations in the dataset. We hypothesize that this is due to GenPlan’s more effective joint optimization process. In practice, LEAP’s sampling process may lead to misalignment between generated actions and goals, even with an oracle for the goal sequence (see figure 3).

Ablation Studies. We assess the significance of various components of GenPlan, results are presented in Table 3.

Joint Prediction ($\mathcal{L}_s + \mathcal{L}_g$). This integration of goal generation (\mathcal{L}_g) with state sequence denoising (\mathcal{L}_s) enhances IC performance and prevents stalling in TP tasks. Without state denoising, the agent tends to exhibit stalling actions as the agent may get stuck in a local region. On the other hand, without \mathcal{L}_g , the agent lacks awareness of sub-tasks associated with the overall task. This is evident in the performance drops observed in the **KeyCorS3R3** and **DoorsOrder** experiments in Table 3, where the agent struggles to achieve sub-goals like key collection or correctly identifying the door sequence.

Entropy. Entropy acts as a regularizer while minimizing the trajectory’s energy. LEAP often gets stuck in local minima when recovering trajectories, leading to the hallucination of actions from demonstrations, such as constantly moving forward or performing in-place turns. The impact of entropy is particularly significant in AP tasks, where the agent navigates more complex environments. This is evident in the performance drops observed in the **MazeClose** environment. However, in IC tasks, where additional actions like “*open*” or “*pickup*” are required, entropy often hinders performance, making it less suitable for such scenarios.

Noise Schedule. In Tables 1 and 2, we compare the use of uniform interpolants versus masking. While masking interpolants generally outperform uniform interpolants in most tasks, the latter succeed in some larger environments. This success is attributed to the inherent randomness in the denoising process, as discussed in Section 4. With masking, the model more easily identifies jumps, simplifying the training. This is also reflected through faster convergence (training) of masked interpolants.

Discussion. Unlike baselines that rely on an oracle for goal positions—often unavailable in real-world scenar-

Attribute	GenPlan-M	Reduction	LEAP \ominus GC
MazeS4G2 (TP)			
w/o JP	32%	\downarrow 7.6%	
w/o Entropy	34.4%	\downarrow 5.2%	20%
KeyCorS3R3 (IC)			
w/o JP	13.6%	\downarrow 4%	
w/o Entropy	7.6%	\downarrow 10%	0%
w/o History	0.4%	\downarrow 17.2%	0%
DoorsOrder (IC)			
w/o JP	15.6%	\downarrow 19.6%	
w/o Entropy	34.4%	\downarrow 0.8%	11%
SeqS5R2Un (AP)			
w/o JP	32.8%	\downarrow 9.2%	
w/o Entropy	34.8%	\downarrow 7.2%	29.2%

Table 3: **Ablation.** The values represent the mean success rates as detailed in Section 5, with reductions shown relative to the results in Tables 1 and 2.

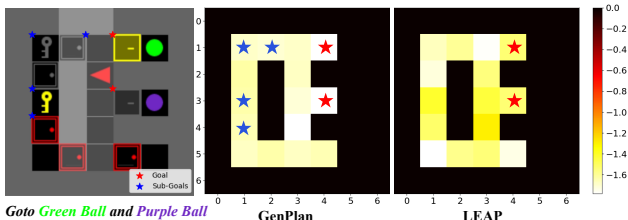


Figure 3: **Energy Landscape.** GenPlan, when conditioned on sub-goals, implicitly assigns minimal energy to necessary sub-goals (e.g., picking up keys, opening doors) for task completion. States closer to the white region are more likely to be transitioned into. LEAP, in contrast, does not prioritize these sub-tasks.

ios—the goal generation module in GenPlan dynamically updates sub-goals, enabling better state coverage (see Appendix A) and unconditional rollouts, where baselines fail to explore certain regions even with oracle guidance. To further illustrate these advantages, we present results on training progression through the learned energy landscape, mission success rates as a function of iterations, and the impact of environment stochasticity (see Appendix A).

Continuous Tasks

We evaluate the models on continuous manipulation tasks: (a) PushT (Florence et al. 2021) and (b) Franka Kitchen (Gupta et al. 2019). Both tasks use state-based variants in continuous manipulator environments. The PushT task assesses task comprehension in unconditional rollouts, with performance measured by final coverage, defined as the IoU between the T-block and the target position. The Franka Kitchen task involves seven possible subtasks, where each demonstration trajectory completes a subset of four in some order. It evaluates long-horizon planning, multimodality, and task commitment, where certain baselines may fail due to mode-shifting or incomplete tasks. Both tasks are evaluated in an unconditional rollout setting. For details on the environment setup and implementation, see Appendix D.

Env	Metric	GenPlan-M	DP-C	DP-T	VQ-BeT
PushT	IoU	0.73	0.73	0.74	0.68
Kitchen	# Tasks	3.40	2.62	3.44	3.66

Table 4: **Quantitative results.** Comparison of baselines on unconditional continuous-space tasks.

Baselines. For our evaluations, we compare GenPlan-M with several baselines to highlight its performance in continuous tasks. GenPlan-M retrieves continuous actions by learning a categorical distribution over discrete latent codes, with corresponding offsets, similar to the Vector Quantized Behavior Transformer (VQ-BeT) (Lee et al. 2024).

Unlike VQ-BeT, which employs a behavior cloning objective, GenPlan-M uses an energy-based loss (see Section 4) and DFM sampling with causal masks, providing greater flexibility and improved generalization. Additionally, we benchmark against Diffusion Policy (DP), a state-of-the-art behavior cloning method, evaluating both its CNN-based (DP-C) and Transformer-based (DP-T) variants. For model and environment hyperparameters, we adopt the configurations from (Lee et al. 2024).

Results. GenPlan-M demonstrates competitive performance against state-of-the-art behavior cloning approaches. While diffusion policies excel at low-level tasks such as PushT, GenPlan-M, and VQ-BeT outperforms the diffusion-based approach (DP-C) in the Kitchen environment, where diffusion falls behind by an entire subtask. These results highlight the advantages of modeling with categorical distributions for multi-task missions and unconditional planning.

6 Conclusion

We study the problem of learning to plan from demonstrations, particularly for unseen tasks and environments. We propose GenPlan, an energy-DFM-based planner that learns annealed energy landscapes and uses DFM sampling to iteratively denoise plans. Through simulation studies, we demonstrate how joint energy-based denoising improves performance in complex and long-horizon tasks.

Limitations. (1) The entropy lower bound β in eq. 4b is currently a hyper-parameter that must be manually specified. (2) We assume access to near-optimal demonstration trajectories for training (Section 5); however, this assumption may not hold in all settings. Initial results show that GenPlan performs well even when trained on datasets with a mixture of sub-optimal demonstrations (Appendix E). However, further studies are needed to assess its robustness to sub-optimality in demonstrations.

Future Work. To address the above limitations, we plan to extend GenPlan for online fine-tuning via hindsight experience replay (Zheng, Zhang, and Grover 2022; Furuta, Matsuo, and Gu 2022). Additionally, GenPlan offers a flexible and scalable framework that can be extended to multi-agent learning settings (Meng et al. 2022).

Acknowledgments

This research is supported by the Natural Sciences and Engineering Research Council of Canada (NSERC) and by the Vector Scholarship in Artificial Intelligence, provided through the Vector Institute.

References

- Campbell, A.; Benton, J.; De Bortoli, V.; Rainforth, T.; Deligiannidis, G.; and Doucet, A. 2022. A continuous time framework for discrete denoising models. *Advances in Neural Information Processing Systems*.
- Campbell, A.; Yim, J.; Barzilay, R.; Rainforth, T.; and Jaakkola, T. 2024. Generative Flows on Discrete State-Spaces: Enabling Multimodal Flows with Applications to Protein Co-Design. *arXiv:2402.04997*.
- Chen, H.; Du, Y.; Chen, Y.; Tenenbaum, J. B.; and Vela, P. A. 2023. Planning with Sequence Models through Iterative Energy Minimization. In *ICLR*.
- Chen, L.; Lu, K.; Rajeswaran, A.; Lee, K.; Grover, A.; Laskin, M.; Abbeel, P.; Srinivas, A.; and Mordatch, I. 2021. Decision Transformer: Reinforcement Learning via Sequence Modeling. In *Advances in Neural Information Processing Systems*, volume 34, 15084–15097.
- Chevalier-Boisvert, M.; Bahdanau, D.; Lahlou, S.; Willems, L.; Saharia, C.; Nguyen, T. H.; and Bengio, Y. 2019. BabyAI: First Steps Towards Grounded Language Learning With a Human In the Loop. In *International Conference on Learning Representations*.
- Chi, C.; Feng, S.; Du, Y.; Xu, Z.; Cousineau, E.; Burchfiel, B.; and Song, S. 2023. Diffusion Policy: Visuomotor Policy Learning via Action Diffusion. *ArXiv:2303.04137* [cs].
- Devlin, J.; Chang, M.-W.; Lee, K.; and Toutanova, K. 2018. Bert: Pre-training of deep bidirectional transformers for language understanding. *arXiv preprint arXiv:1810.04805*.
- Du, Y.; Mao, J.; and Tenenbaum, J. B. 2024. Learning Iterative Reasoning through Energy Diffusion. In *Forty-first International Conference on Machine Learning*.
- Emmons, S.; Eysenbach, B.; Kostrikov, I.; and Levine, S. 2022. RvS: What is Essential for Offline RL via Supervised Learning? In *International Conference on Learning Representations*.
- Eysenbach, B.; Zhang, T.; Levine, S.; and Salakhutdinov, R. 2022. Contrastive Learning as Goal-Conditioned Reinforcement Learning. In Oh, A. H.; Agarwal, A.; Belgrave, D.; and Cho, K., eds., *Advances in Neural Information Processing Systems*.
- Florence, P.; Lynch, C.; Zeng, A.; Ramirez, O.; Wahid, A.; Downs, L.; Wong, A.; Lee, J.; Mordatch, I.; and Tompson, J. 2021. Implicit Behavioral Cloning. *Conference on Robot Learning (CoRL)*.
- Fujimoto, S.; Meger, D.; and Precup, D. 2019. Off-Policy Deep Reinforcement Learning without Exploration. In *International Conference on Machine Learning*, 2052–2062.
- Furuta, H.; Matsuo, Y.; and Gu, S. S. 2022. Generalized Decision Transformer for Offline Hindsight Information Matching. In *International Conference on Learning Representations*.
- Goyal, K.; Dyer, C.; and Berg-Kirkpatrick, T. 2021. Exposing the Implicit Energy Networks behind Masked Language Models via Metropolis–Hastings. *arXiv preprint arXiv:2106.02736*.
- Gupta, A.; Kumar, V.; Lynch, C.; Levine, S.; and Hausman, K. 2019. Relay policy learning: Solving long-horizon tasks via imitation and reinforcement learning. *arXiv preprint arXiv:1910.11956*.
- Haarnoja, T.; Tang, H.; Abbeel, P.; and Levine, S. 2017. Reinforcement Learning with Deep Energy-Based Policies. *arXiv:1702.08165*.
- Ho, J.; Jain, A.; and Abbeel, P. 2020. Denoising Diffusion Probabilistic Models. *arXiv:2006.11239*.
- Janner, M.; Du, Y.; Tenenbaum, J. B.; and Levine, S. 2022. Planning with Diffusion for Flexible Behavior Synthesis. *arXiv:2205.09991*.
- Janner, M.; Li, Q.; and Levine, S. 2021. Offline Reinforcement Learning as One Big Sequence Modeling Problem.
- Kostrikov, I.; Nair, A.; and Levine, S. 2021. Offline reinforcement learning with implicit q-learning. *arXiv preprint arXiv:2110.06169*.
- Kumar, A.; Fu, J.; Soh, M.; Tucker, G.; and Levine, S. 2019. Stabilizing off-policy q-learning via bootstrapping error reduction. *Advances in Neural Information Processing Systems*, 32.
- Lambert, N.; Pister, K.; and Calandra, R. 2022. Investigating Compounding Prediction Errors in Learned Dynamics Models. *arXiv:2203.09637*.
- Lee, S.; Wang, Y.; Etukuru, H.; Kim, H. J.; Shafiuallah, N. M. M.; and Pinto, L. 2024. Behavior Generation with Latent Actions. *arXiv preprint arXiv:2403.03181*.
- Levine, S.; Kumar, A.; Tucker, G.; and Fu, J. 2020. Offline Reinforcement Learning: Tutorial, Review, and Perspectives on Open Problems. *arXiv:2005.01643*.
- Meng, L.; Wen, M.; Yang, Y.; Le, C.; Li, X.; Zhang, W.; Wen, Y.; Zhang, H.; Wang, J.; and Xu, B. 2022. Offline Pre-trained Multi-Agent Decision Transformer: One Big Sequence Model Tackles All SMAC Tasks. *arXiv:2112.02845*.
- Perez, E.; Strub, F.; De Vries, H.; Dumoulin, V.; and Courville, A. 2018. Film: Visual reasoning with a general conditioning layer. In *Proceedings of the AAAI Conference on Artificial Intelligence*.
- Schmidhuber, J. 2020. Reinforcement Learning Upside Down: Don’t Predict Rewards – Just Map Them to Actions. *arXiv:1912.02875*.
- Schmied, T.; Hofmarcher, M.; Paischer, F.; Pascanu, R.; and Hochreiter, S. 2023. Learning to Modulate pre-trained Models in RL. In *Thirty-seventh Conference on Neural Information Processing Systems*.
- Sun, J.; Huang, D.-A.; Lu, B.; Liu, Y.-H.; Zhou, B.; and Garg, A. 2022. PlaTe: Visually-Grounded Planning With Transformers in Procedural Tasks. *IEEE Robotics and Automation Letters*, 7(2): 4924–4930.
- Yu, T.; Thomas, G.; Yu, L.; Ermon, S.; Zou, J.; Levine, S.; Finn, C.; and Ma, T. 2020. MOPO: Model-based Offline Policy Optimization. *arXiv preprint arXiv:2005.13239*.

Zheng, Q.; Zhang, A.; and Grover, A. 2022. Online decision transformer. In *International Conference on Machine Learning*. PMLR.

Appendix

Organization of Appendix

The Appendix is organized as follows: Appendix A provides implementation details for the BabyAI environment. This is followed by additional results and discussions in Appendix B. Ablation and comparative studies on objective and optimization methods are presented in Appendix C. Details of the continuous tasks are outlined in Appendix D, while Appendix E includes further experiments on zero-shot adaption to different tasks in MetaWorld. Finally, Appendix F briefly discusses sampling and the choice of the rate matrix in Algorithm 2.

A BabyAI Implementation Details

Input and Networks.

The various inputs and their corresponding dimensions are presented in Table 5 for the BabyAI environments. We construct GenPlan following the transformer architecture (with bi-directional masks) described in (Chi et al. 2023). The inputs to the model include token embeddings for observations, states, and actions, which are generated through specific mappings. Detailed illustrations of these mappings can be found in Figures 2 and 7.

$$FiLM(I_{\text{ctx}}, s_{\text{ctx}}, \xi, t, k) \rightarrow \text{tok}_o \quad f_{\theta_s}(\mathbf{s}_k^t) \rightarrow \text{tok}_s \quad f_{\theta_a}(\mathbf{a}_k^t) \rightarrow \text{tok}_a$$

The observation token tok_o is obtained from the panoramic image I , state s_{ctx} , instruction ξ , and timestep t in the CTMC. The FiLM (Feature-wise Linear Modulation) function (Perez et al. 2018) transforms these inputs into an observation embedding. Note that, in the case of a masked or corrupt state, these observation tokens are set to zero during training. We follow the same instruction encoder as used in the BabyAI agent model (Chevalier-Boisvert et al. 2019). The context length, ctx (see Table 8), acts as a memory for the agent and provides past trajectories of length ctx . This embedding, along with the corrupted state \mathbf{s}_k^t and action \mathbf{a}_k^t tokens generated by the embedding networks f_{θ_s} and f_{θ_a} , is fed into the transformer’s decoder stack. The transformer’s cross-attention mechanism is employed in this joint denoising process. The decoder then predicts the true labels $\mathbf{s}^1, \mathbf{g}^1$, and \mathbf{a}^1 , with the observation tokens guiding the denoising process (figure 2). Consequently, we have $H + 1$ tokens in the cross-attention module, where the $+1$ corresponds to the CTMC timestep-based embedding, and $2H$ tokens serve as input to the transformer’s decoder block. Further details on the input dimensions and the architecture are provided in Table 6.

Input	Vector Space	Description
Image I	$\mathbb{R}^{S \times S \times 3}$	Symbolic representation of env. S (size of env.)
State s_k^t	\mathbb{R}^3	Tuple corresponding to $\langle x, y, \text{dir} \rangle$
Goal g_k^t	$\mathbb{R}^{\Pi \times 2}$	No. of goals (Π), each with x, y positions
Instructions ξ	—	Task-specific instructions
Actions a_k^t	\mathbb{R}^6	Discrete set of actions available

Table 5: **Offline data.** Various components of the trajectory.

Environments.

Detailed settings for the BabyAI environments are provided in Table 7. We evaluate across three task paradigms as described in Section 5, with tasks in IC and AP being particularly challenging. For instance, in the **BlockUnlock** task, the agent must first remove an obstacle by picking it up and repositioning it, then retrieve a key to unlock the door, and finally navigate to the goal, which is always located in the locked room. Due to the order-critical nature of these tasks, we observe that only GenPlan succeeds, while other baselines fail. Similarly, in AP tasks, the agent must generalize to more complex environments than those encountered during training. For further details, refer to Figures 4, 5, and 6.

Baseline Models.

We use the official implementations for both LEAP (Chen et al. 2023) and DT (Chen et al. 2021). To address the limitations of their maximum likelihood objective, which fails to generalize in predicting novel goals (e.g., consistently predicting goals as the corner cells), we augment these baselines with simulator-based goal conditioning. The BabyAI simulator is used to obtain the final goal and sub-goals for goal-conditioned planning in the baseline models. All models are trained in an end-to-end fashion.

B Additional Results and Discussion.

We present additional experiments to further evaluate GenPlan’s capabilities across various scenarios. These include analyses of coverage, iterative denoising, energy landscapes, convergence rates, and entropy, along with performance in stochastic environments and sub-optimal data. These experiments provide additional insights into GenPlan’s generalizability, robustness, and ability to adapt to diverse and complex tasks.

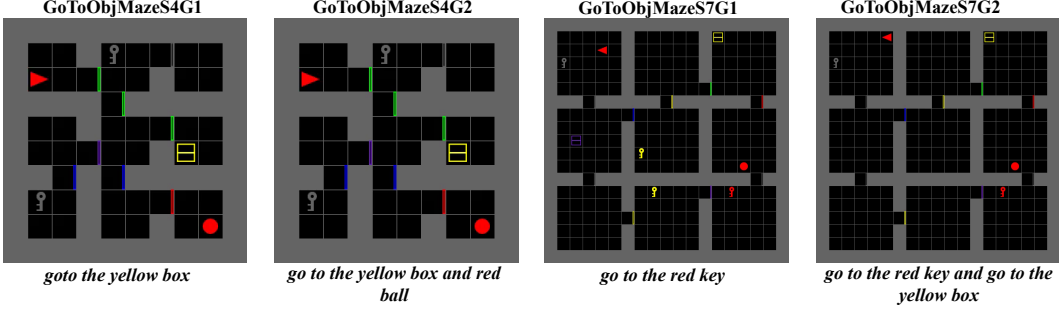


Figure 4: **Trajectory Planning (TP).** The agent is randomly initialized and must navigate through a maze-like environment to reach the goal(s). In each evaluation, the map layout, the agent's initial position, and goal positions are varied. Note that in the case of GenPlan, the agent does not have access to the ground truth goal positions, whereas other baselines do.

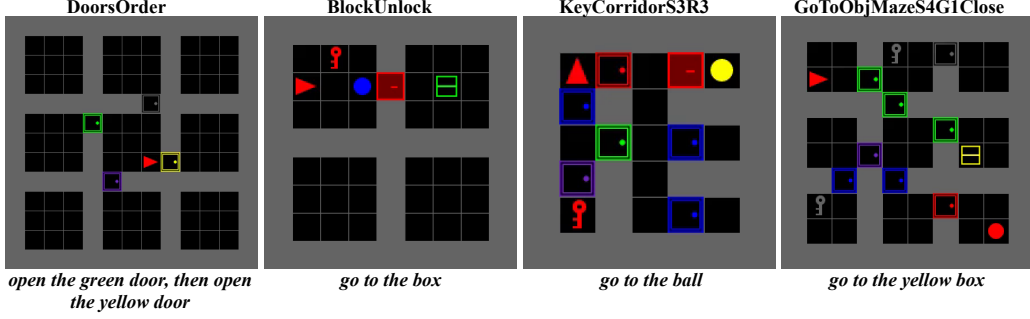


Figure 5: **Instruction Completion IC.** These tasks are more complex than TP, requiring the agent to perform additional actions such as *pickup*, *drop*, and *open* in addition to navigation. For example, in *DoorsOpen*, the agent must open the specified doors in the correct order without accidentally entering other rooms.

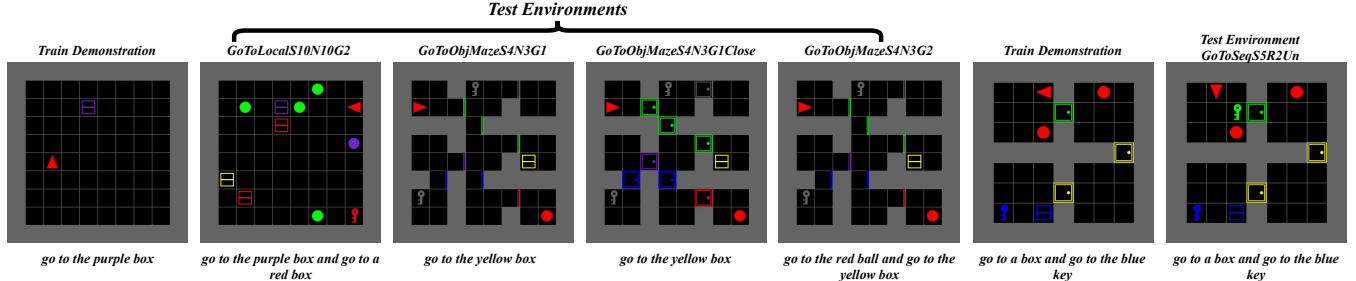


Figure 6: **Adaptive Planning AP.** The model is trained on simpler tasks and tested for adaptability by progressively increasing task difficulty. In *GoToObjMazeClose* and *GoToSeqUn*, we evaluate whether the model can demonstrate novel skills, such as unblocking obstacles and opening doors.

Hyperparameter	Value
Number of layers	4
Number of attention heads	4
Embedding dimension	128
Batch size	64
Image Encoder	nn.Conv2d
Image Encoder channels	128, 128
Image Encoder filter sizes	$2 \times 2, 3 \times 3$
Image Encoder maxpool strides	2, 2 (Image Encoder may vary a little depending on the environment size)
Instruction Encoder	nn.GRU
Instruction Encoder channels	128
State Encoder	nn.Linear
State Encoder channels	128, 128, 128
Max epochs	400
Dropout	0.1
Learning rate	$8 * 10^{-4}$
Adam betas	(0.9, 0.95)
Grad norm clip	1.0
Weight decay	0.1
Learning rate decay	Linear warmup and cosine decay (see code for details)

Table 6: Hyperparameters of GenPlan for BabyAI experiments.

Task	Env	Size	# Room	# Obs	Door	Unblocking	Max Steps
Task Planning (TP)	GoToObjMazeS4G1	10×10	9	4	Open	No	399
	GoToObjMazeS4G2	10×10	9	4	Open	No	499
	GoToObjMazeS7G1	19×19	9	7	Open	No	699
	GoToObjMazeS7G2	19×19	9	7	Open	No	999
Instruction Completion (IC)	GoToObjMazeClose	10×10	9	4	Closed	No	499
	DoorsOrder	13×13	9	0	Closed	No	144
	BlockUnlock	8×8	2	2	Closed	Yes	399
	KeyCorridorS3R3	7×7	6	2	Closed	No	499
Adaptive Planning (AP)	GoToLocalS10N10G2	10×10	10	4	Open	No	299
	GoToObjMazeS4N3G1	10×10	9	4	Open	No	499
	GoToObjMazeClose	10×10	9	4	Closed	No	499
	GoToSeqS5R2Un	9×9	4	5	Closed	Yes	499

Table 7: BabyAI environment setting details.

Coverage. We perform coverage experiments on both adaptive planning (AP) and trajectory planning (TP) tasks in novel environments. For both tasks, we evaluate models across unseen environments where the map layout (fixed) was not observed during training, and the goal position is randomized to different rooms. The results, shown in figure 8, report the coverage and success rates for each model.

In AP tasks, where both the task and environment are novel, the agent is trained on a planar goal-conditioned task (without walls) and must adapt to a maze structure in a zero-shot setting. As illustrated in figure 8, GenPlan significantly outperforms the baselines due to its goal generation module (Section 4), which effectively proposes sub-goals and goal regions, providing clear guidance. In contrast, baseline models struggle with ambiguous guidance (figure 3), often leading to agent stalling, even with access to the simulator for ground truth. GenPlan demonstrates efficient exploration and strong generalizability in these settings.

For TP tasks, we evaluate the models’ trajectory planning capabilities in a maze-goal-reaching task with unseen maps (figure 9). This setup excludes goal modules (learned or oracle) and focuses solely on trajectory planning. Given the map and instructions, GenPlan successfully plans trajectories, even when initializing goals in different rooms. In comparison, baseline models struggle, with DT performing competitively in generalizing to the same task but facing significant challenges in adaptation. GenPlan consistently outperforms baselines in both generalization and adaptation tasks.

Effect of Iterative Denoising. At inference, the number of denoising steps for planning is determined independent of training (Algorithm 2), enabling post-hoc adaptations with various rate samplers. For harder problems, more iterations or better samplers can be used to obtain minimal energy trajectories. From figure 10A, we observe that around $H/2$ iterations provide good results, allowing approximately two dimensions to transition simultaneously in a single step.

Env	Context	Plan	GenPlan		LEAP Iteration
			Iteration	Entropy	
GoToObjMazeS4G1	1	10	5	0.3	10
GoToObjMazeS4G2	1	10	5	0.3	10
GoToObjMazeS7G1	1	20	10	0.3	50
GoToObjMazeS7G2	1	20	10	0.3	50
GoToObjMazeClose	1	10	5	0.3	10
DoorsOrder	1	10	5	0.3	10
BlockUnlock	10	30	15	0.3	50
KeyCorridorS3R3	10	30	15	0.3	50
GoToLocalS10N10G2	1	10	5	0.7	10
GoToObjMazeS4N3G1	1	10	5	0.7	10
GoToObjMazeClose	1	10	5	0.7	10
GoToObjMazeS4G2	1	10	5	0.7	10
GoToSeqS5R2Un	1	20	10	0.7	40

Table 8: **Training Configurations.** For most tasks, planning is based solely on the current state observation and aims to plan for H steps. However, for **KeyCorridor** and **BlockUnlock**, which involve complex sub-tasks and require memory to track completed tasks, context is used.

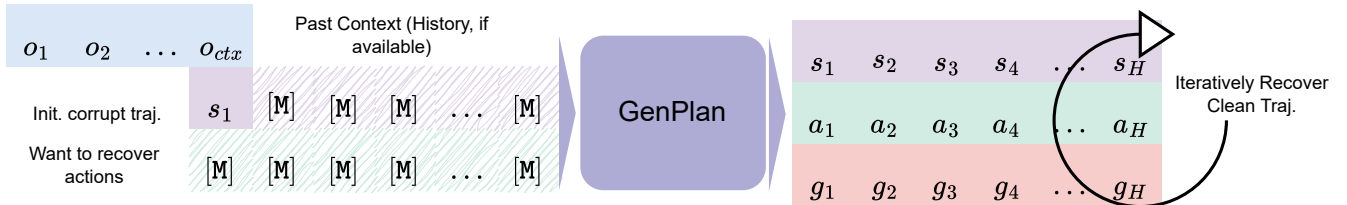


Figure 7: **GenPlan I/O.** During planning, the model takes in a corrupted trajectory along with the current state and past observations (if available), and iteratively recovers the clean trajectory.

Energy Landscape. We investigate the energy assignment to trajectories with varying noise levels throughout training and observe that (a) GenPlan learns to reduce the energy for clean sequences and (b) increases the energy for corrupted trajectories (figure 10B). Since this denoising is done jointly, the energy measure provides an implicit sense of the goodness of an action at a particular state (also see figure 3). This helps verify that the objective in eq. 4a indeed facilitates denoising.

Rate of Convergence DFM. In the masking interpolant, the model easily identifies which indices are corrupted, simplifying the training process. This is evident through faster convergence rates. We report the correct action rate (i.e., the portion of the corrupted trajectory that the model can recover) and observe that masked denoising converges much faster (figure 11A). Consequently, the masked tokens receive the lowest attention scores. In contrast, it is relatively harder for the model to determine which tokens are corrupted in the uniform interpolant, leading to slower convergence.

Entropy. Continuing our discussion from Section 5, we report success rates by varying the entropy lower bound. For TP and IC tasks, we observe that entropy levels above 0.3 offer little benefit. However, for AP tasks, we set the entropy to 0.7, as this facilitates task discovery (i.e., performing novel actions that are absent from the dataset) (see figure 11B).

We extend the results presented in Table 2 by introducing an additional variant, **LEAP \ominus GC**. Similar to GenPlan, this variant of LEAP incorporates a lower bound on entropy, facilitating novel task adaptation.

Environment	Unconditional Rollouts				Conditional Rollouts	
	GenPlan-U	GenPlan-M	LEAP \ominus GC	LEAP \oplus GC	LEAP	DT
	Adaptive Planning (AP)					
GoToLocalS10N10G2	82.4%	88%	76%	69.2%	78%	25.6%
GoToObjMazeS4N3G1	56%	62%	44.8%	52%	48%	24%
GoToObjMazeClose	31.2%	34.8%	10%	16.4%	10%	8.8%
GoToObjMazeS4G2	28.8%	34.8%	14%	21.2%	18.4%	3.6%
GoToSeqS5R2Un	35.6%	42%	29.2%	30.8%	38%	29.2%
AP Mean (13.84\uparrow)	46.8%	52.32%	34.8%	37.92%	38.48%	18.24%

Table 9: **BabyAI quantitative performance.** Success rates of the models across different environments are presented. The abbreviations **SW**, **NX**, **RY**, and **GZ** in the environment names represent the size (**W**) of a room in the map, the number of obstacles (**X**), the number of rows (**Y**), and the number of goals (**Z**) during testing, respectively. See Appendix A for more details.

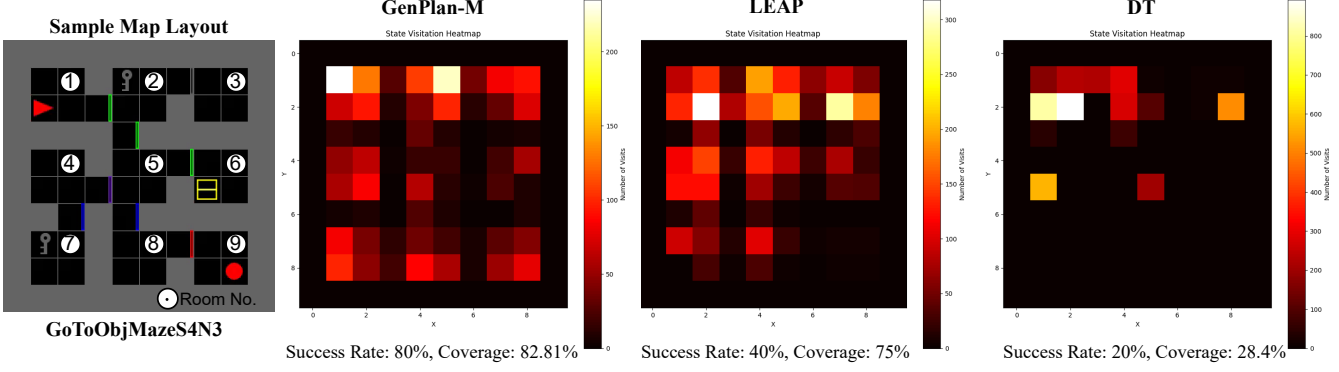


Figure 8: **State Coverage (AP).** State visit frequency is evaluated across 10 unseen maze layouts with varying goal positions (Rooms 1-9), starting from a fixed agent position (Room 1).

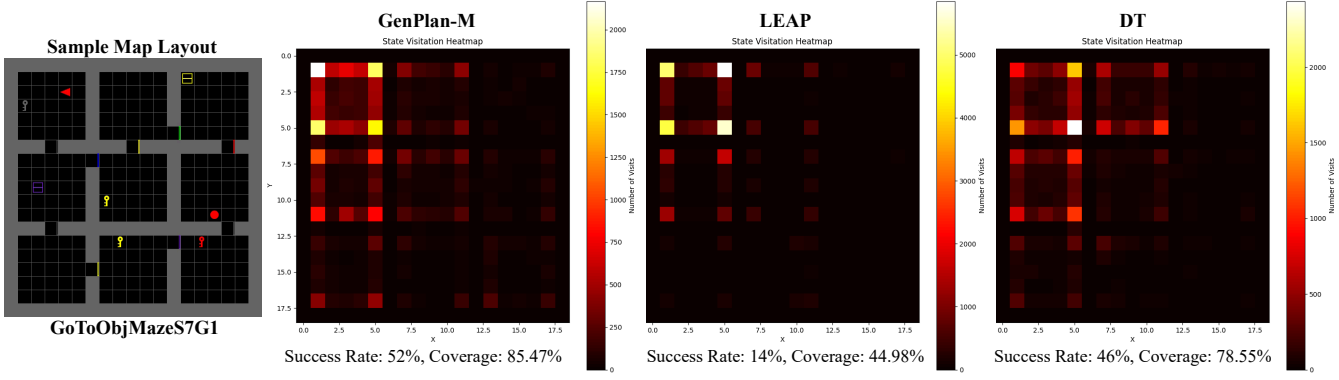


Figure 9: **State Coverage (TP).** Coverage is evaluated in larger environments. Results are reported across 50 map variations from a fixed start position (Room 1).

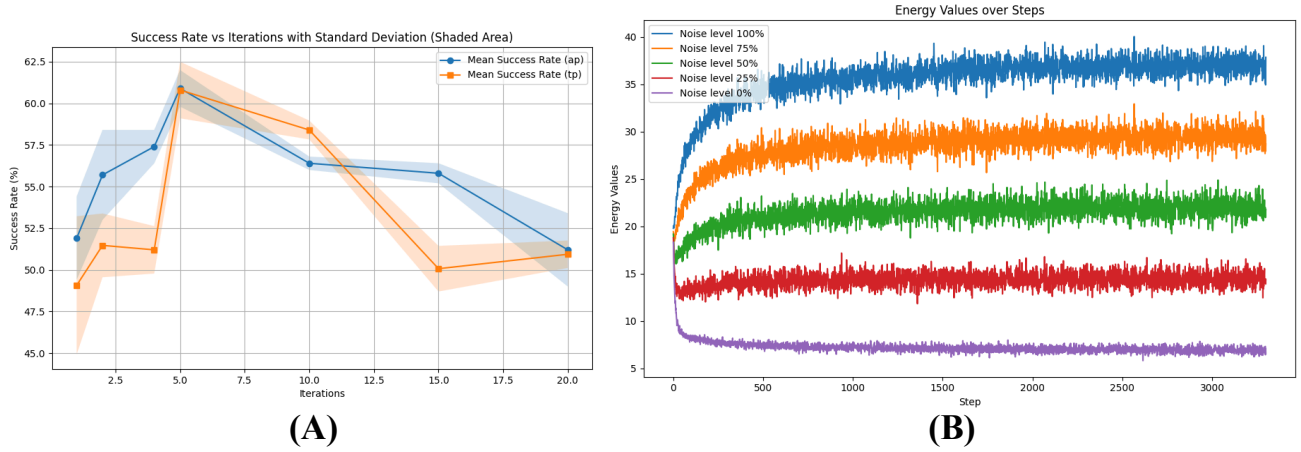


Figure 10: **GenPlan Analysis.** (A) Success rate as a function of the number of denoising iterations, reported using 3 different training seeds evaluated on 250 environments, specifically for *GoToObjMazeS4N3G1* (*AP*) and *GoToObjMazeS4G1* (*TP*). (B) Energy landscape learned by GenPlan during training, illustrating that GenPlan effectively captures the true action distribution by assigning low energy to noise-free sequences.

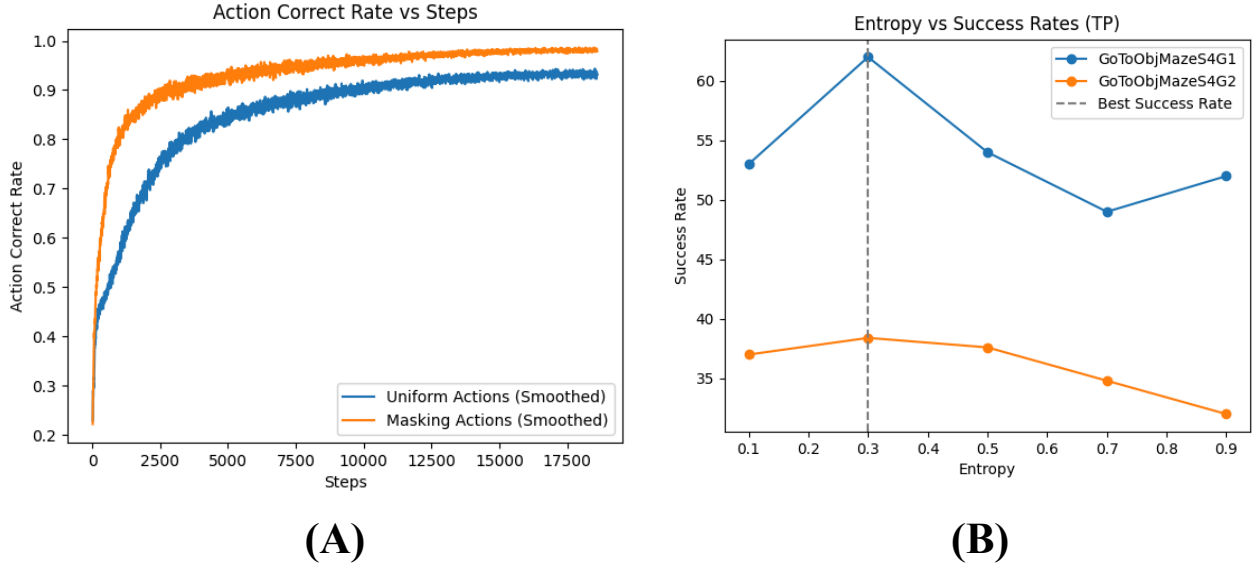


Figure 11: **GenPlan Configurations.** (A) Training progression of GenPlan, showing that GenPlan-M converges faster than GenPlan-U. (B) Success rate as a function of entropy.

Stochasticity in Environments. In this setup, the agent operates in an environment where it has a 20% chance that its chosen action (e.g., left or right) will be randomly mapped to another action with uniform probability. To address these stochastic settings, we replan after each step using single-step rollouts, unlike the multi-step rollouts used in the settings presented in Tables 1 and 2. We apply the same replanning strategy to the baseline models for a fair comparison.

The results in Table 10 show that GenPlan performs on par with baseline methods in stochastic environments, where both use feedback at each step. However, in adaptive environments, even with feedback, the baseline model (DT) fails, while GenPlan and LEAP succeed.

Env	GenPlan-M	LEAP	DT
GoToObjMazeS7G1 (TP)	48%	18%	52%
GoToObjMazeS4N3G1 (AP)	54.8%	52%	23.2%

Table 10: **Stochastic Environments.** Success rates of models in task planning and adaptive environments using single-step rollouts to account for stochasticity.

Context Length. We use context length as a memory mechanism for tracking completed sub-goals, which is primarily beneficial in tasks like **KeyCorridorS3R3** and **BlockUnlock** (Table 1). While most TP tasks and multi-objective IC tasks operate under a Markovian assumption, these tasks involve complex sub-tasks requiring memory to track progress. Context-based planning is also enabled for baselines (see figure 7)

Time considerations. We observe that due to the MLM objective in LEAP, they must sequentially mask each action, which is time-consuming. Additionally, gradients are updated only after accumulating losses from all action tokens in the horizon, making the process memory-intensive. In contrast, GenPlan controls the number of masked tokens using the CTMC timestep t , eliminating the need for sequential masking and saving significant time. Although GenPlan is slightly slower than DT due to its iterative inference process and the bi-directional mask loss taking longer than the causal masks in DT, it still performs within a reasonable time frame. The total training and inference times are reported in Table 11.

Mode	Env	GenPlan-M	LEAP	DT
Train	GoToObjMazeS4G2	34m	5hrs	30min
	GoToObjMazeS7G2	1hr 3min	6hrs	57min
Eval	GoToObjMazeS4	3mins	10min	2min
	GoToObjMazeS7	18min	36min	10min

Table 11: Comparison of training and evaluation times across different environments and methods. Training is performed with a batch size of 64 over 500 epochs, while evaluation is conducted across 250 environments.

Instructions Ablation. We observe that image inputs play a significant role in learning goal distributions. The training data comprises standalone examples of single goals or skills, while testing involves skill chaining based on prompts in a fully observable environment. GenPlan addresses these challenging tasks by learning energy landscapes and employing DFM sampling.

Prompts are essential in instruction-completion tasks. Procedurally generated by MiniGrid environments, these prompts are available during both training and testing phases. To evaluate their significance, we ablate the instruction embeddings, which are key to instruction completion as seen in Table 12. While the primary focus of this work is to adopt discrete representations for planning with sub-tasks, language grounding is left for future exploration.

Environment	Success Rate	Reduction
Doors Order (IC)	22%	13.2% ↓
GoToLocal10G2 (AP)	73%	15% ↓

Table 12: **Instruction Prompt Ablation.** We ablate the instruction embeddings from the input to assess their significance, as evidenced by the reduction in success rates across environments.

Suboptimal Data. We evaluate the performance of our model when trained on suboptimal data and observe that GenPlan-M retains its generalization capability, while DT fails to adapt effectively. We hypothesize that this is due to the MLE objective in DT being unable to stitch trajectories.

Environment	Optimal Data		Suboptimal Data (25%)	
	GenPlan-M	DT	GenPlan-M	DT
GoToObjMazeS4G1	62%	44%	55.2%	44%
GoToObjMazeS7G1	44.8%	40%	38.8%	15.2%
BlockUnlock	16%	0%	8%	0%

Table 13: **Performance with Suboptimal Trajectories.** We introduce 25% random actions into the training data to simulate suboptimal trajectories. Despite this, GenPlan-M demonstrates robust generalization, outperforming DT across all environments.

C Comparisons with Generative Approaches

We evaluate different generative objectives (BC, Noise Contrastive Estimation) and sampling techniques (Random Shooting (RS), Cross-Entropy Method (CEM), MCMC sampling, and energy gradient-guided sampling). The results for the AP and IC tasks are reported in Table 14.

(i) **Denoising Diffusion Probabilistic Models (DDPM)** (Ho, Jain, and Abbeel 2020; Chi et al. 2023) rely on a BC objective thus struggle to generalize to harder tasks, as shown in Example 1. Models trained solely with BC objectives lack distributional fidelity, limiting their ability to adapt to novel scenarios.

(ii) **Energy models** are challenging to sample from due to their reliance on extensive CEM or MCMC cycles and their instability during training (Chi et al. 2023). Additionally, guided sampling in DDPM (using energy gradients) often results in local minima, where low-energy trajectories are gamed through repeating actions frequently observed in the dataset (e.g., repeated forward movements).

We observe that GenPlan significantly outperforms both approaches, as demonstrated in Table 14.

D Continuous Tasks Implementation Details.

Simulation Setup. (i) **PushT** (Florence et al. 2021): The goal is to push a T-block to a target position and orientation using an end-effector controlled via 2D velocity. The dataset includes 206 human demonstrations. (ii) **Kitchen** (Gupta et al. 2019): A robotic manipulation task with a Franka Panda arm (7D action space) and 566 demonstrations. It comprises 7 sub-tasks, with each trajectory completing 4 tasks in some order. At test time, the metric is the number of tasks completed in an unconditional rollout. Both tasks are evaluated in state space variants.

Sampling / Objective		GoToObjMazeS4G1	KeyCorridorS3R3	DoorsOrder
Energy Models	Random	29.2%	2.8%	26%
	CEM	38.9%	6.4%	28.4%
DDPM	Diffusion BC	25.2%	0.8%	29.2%
	Energy (Gradient)	2%	0%	0%
GenPlan	Energy+DFM	62%	17.6%	35.2%

Table 14: **Comparison of Energy-Based and DDPM Baselines on MiniGrid Tasks.** We compare various sampling techniques and generative objectives on discrete planning tasks. GenPlan demonstrates significant improvements in success rates, particularly on more complex tasks, by combining energy objectives with DFM sampling.



Env	Metric	GenPlan-M	VQ-BeT	DP-C	DP-T
PushT	Final Coverage	0.73	0.7	0.73	0.74
	Max Coverage	0.77	0.73	0.86	0.83
Kitchen	# Tasks	3.40	3.66	2.62	3.44

Table 16: **PushT Task Evaluation.** Comparison of state-based and image-based policies.

Table 15: **PushT env.**

Evaluation metrics include final and maximum coverage, measured by the Intersection over Union (IoU) between the T-block and the target T position.

We compare our approach with VQ-BeT (Lee et al. 2024), which employs a categorical transformer-based model to infer action codes, subsequently decoded using a pre-trained motion primitive model (VQ-VAE). In our experiments, we use the same pre-trained motion primitive but replace the auto-regressive transformer with GenPlan’s objective and sampling process.

E MetaWorld Implementation Details.

We assess the adaptive capabilities of the agents in MetaWorld’s unseen tasks.

Simulation Setup. Our simulation setup closely follows that of (Schmied et al. 2023), benchmarking GenPlan on MetaWorld tasks that encompass various robotic manipulation challenges. Both MDDT (Schmied et al. 2023) and GenPlan are trained on five tasks (In-Dist.) and evaluated on nine tasks, including four new tasks (Out-Dist.) designed to test adaptation. Consistent with the BabyAI experiments, we directly evaluate zero-shot performance. Each episode consists of 200 timesteps per task, and we report success rates and mean rewards across Meta-World experiments.

To enable multi-domain learning and task adaptation, the action space is modeled as a categorical distribution with actions discretized into 64 bins using min-max tokenization, as in (Schmied et al. 2023). In MetaWorld, the state and action spaces are consistent across environments ($|S| = 39$, $|A| = 4$). The dataset comprises 10K trajectories per task (length 200) collected by task-specific Soft Actor Critic (SAC) agents, featuring behavior ranging from random to expert-level. Unlike the near-optimal demonstrations in BabyAI, this dataset offers broader variability. Sequential action prediction with a planning horizon of 1 is employed, which provides feedback at each step and improves adaptive performance. The environments are detailed in Table 18.

Category	Metric	MDDT	GenPlan-M
In-Dist.	SR	0.88 ± 0.032	0.786 ± 0.104
	MR	1566 ± 38.0	1465.66 ± 34.79
Out-Dist.	SR	0.3 ± 0.081	0.333 ± 0.047
	MR	617 ± 52.46	620.33 ± 48.58

Table 17: **Quantitative Performance.** Comparison between MDDT and GenPlan. Success rates (SR) and mean rewards (MR) are reported across three unique seeds.

Rollout. During evaluation, actions are sequentially predicted token by token to fill the 4-dimensional action space ($|A| = 4$). After completing the action, the corresponding observation is obtained (plan horizon of 1).

Baselines and Results. We follow the pre-processing steps from MDDT (Schmied et al. 2023), with GenPlan utilizing a flow-based generative loss instead of the auto-regressive loss, as described in Section 4. During sampling, return-conditioned sampling (Chen et al. 2021) is used. While MDDT performs well on in-distribution tasks, GenPlan demonstrates superior

Task	\mathcal{S}	\mathcal{A}	Dataset		Evaluation - SR	
			SR	Reward	GenPlan	MDDT
In Dist. Environments						
button-press-v2	39	4	1.0	1430.44	0.73±0.11	0.8±0.2
dial-turn-v2	39	4	0.8	1674.29	0.86±0.23	0.93±0.11
disassemble-v2	39	4	1.0	1396.55	0.66±0	0.8±0.2
plate-slide-v2	39	4	1.0	1667.35	1±0	1±0
reach-v2	39	4	1.0	1858.99	0.73±0.11	0.933±0.11
Adaptive Environments (Out Dist.)						
reach-wall-v2	39	4	1.0	1831.14	0.86±0.11	0.73 ±0.11
plate-slide-side-v2	39	4	1.0	1663.35	0±0	0±0
button-press-wall-v2	39	4	1.0	1508.16	0.46±0.11	0.4±0.2
coffee-button-v2	39	4	1.0	1499.17	0.13±0.067	0.2±0.2

Table 18: **Dataset and Performance Scores.** The agent is trained only on datasets from the 5 in-distribution environments and evaluated on all nine. Datasets from adaptive environments are not used.

generalization to closely related tasks (e.g., *reach* and *button* tasks) and adapts effectively to variations in orientation or axis without fine-tuning.

The masking variant of GenPlan benefits from a robust training process and multi-modality by predicting alternate actions at corrupt timesteps in the trajectory. As a result, GenPlan achieves slightly better scores in adaptive tasks.

F Rate Matrices and Sampling

t	k_1	k_2	k_3	k_4	k_5	k_6	k_7	k_8	k_9	k_{10}
0.0	6	6	6	6	6	6	6	6	6	6
0.2	1	6	6	0	6	5	6	6	6	6
0.4	1	6	6	0	6	5	6	6	2	6
0.6	1	5	6	0	6	5	6	6	2	6
0.8	1	5	0	0	2	5	1	1	2	2
1.0	1	5	0	0	2	5	1	1	2	2

Table 19: **Masking Interpolant.** The sample is initialized with the mask state (represented by 6) and iteratively denoised to obtain the clean sequence (in green).

t	k_1	k_2	k_3	k_4	k_5	k_6	k_7	k_8	k_9	k_{10}
0.0	3	5	4	3	2	4	1	2	0	2
0.2	3	5	4	0	2	4	1	2	0	2
0.4	3	5	4	0	2	4	1	2	2	2
0.6	1	5	0	0	2	4	1	1	2	2
0.8	1	5	0	0	2	5	1	1	2	2
1.0	1	5	0	0	2	5	1	1	2	2

Table 20: **Uniform Interpolant.** The sample is initialized with uniform noise (in red) and iteratively denoised to obtain the clean trajectory (in green).

Once the denoising model $p_{1|t}^\theta$ is trained, we can select a rate matrix to simulate the CTMC for generating samples (see Algorithm 2). Campbell et al. proposes the following rate matrix definition as an initial choice (for simplicity, consider the case where $H = 1$):

$$R_t^*(x_k^t, j_k | x_k^1) := \frac{\text{ReLU}(\partial_t p_{t|1}(j_k | x_k^1) - \partial_t p_{t|1}(x_k^t | x_k^1))}{\mathcal{Z}_t p_{t|1}(x_k^t | x_k^1)},$$

where $\text{ReLU}(a) = \max(a, 0)$ and \mathcal{Z}_t is the number of states with non-zero mass at t , defined as $\mathcal{Z}_t = |\{x_k^t : p_{t|1}(x_k^t | x_k^1) > 0\}|$. Note that $R_t^*(x_k^t, j_k | x_k^1) = 0$ when $p_{t|1}(x_k^t | x_k^1) = 0$ or $p_{t|1}(j_k | x_k^1) = 0$. Additionally, when $x_k^t = j_k$, we have $R_t^*(x_k^t, x_k^t | x_k^1) = -\sum_{j_k \neq x_k^t} R_t^*(x_k^t, j_k | x_k^1)$.

To ensure that the rate matrix R_t^* is well-defined and maintains the flow of probability mass between states, we assume that $p_{t|1}(x_k^t | x_k^1) > 0$. This assumption is crucial because it ensures that the state x_k^t is “alive” and carries some probability mass at time t . If $p_{t|1}(x_k^t | x_k^1) = 0$, then $R_t^*(x_k^t, j_k | x_k^1)$ would either be undefined or forced to be zero, as the state would be considered “dead,” unable to either receive or provide any mass. Without this assumption, a state could demand incoming mass without being able to reciprocate, violating the consistency of the conditional flow process and the Kolmogorov equation.